

Pan-Arctic simulation of coupled nutrient-sulfur cycling due to sea ice biology: Preliminary results

S. Elliott,¹ C. Deal,² G. Humphries,³ E. Hunke,¹ N. Jeffery,¹ M. Jin,² M. Levasseur,⁴ and J. Stefels⁵

Received 9 January 2011; revised 8 June 2011; accepted 16 September 2011; published 15 February 2012.

[1] A dynamic model is constructed for interactive silicon, nitrogen, sulfur processing in and below Arctic sea ice, by ecosystems residing in the lower few centimeters of the distributed pack. A biogeochemically active bottom layer supporting sources/sinks for the pennate diatoms is appended to thickness categories of a global sea ice code. Nutrients transfer from the ocean mixed layer to drive algal growth, while sulfur metabolites are reinjected from the ice interface. Freeze, flux, flush and melt processes are linked to multielement geocycling for the entire high-latitude regime. Major element kinetics are optimized initially to reproduce chlorophyll observations, which extend across the seasons. Principal influences on biomass are solute exchange velocity at the solid interface, optical averaging in active ice and cell retention against ablation. The sulfur mechanism encompasses open water features such as accumulation of particulate dimethyl sulfoniopropionate, grazing and other disruptive releases, plus bacterial/enzymatic conversion to volatile dimethyl sulfide. For baseline settings, the mixed layer trace gas distribution matches sparging measurements where they are available. However, concentrations rise to well over 10 nM in remote, unsampled locations. Peak contributions are supported by ice grazing, mortality and fractional melting. The model bottom layer adds substantially to a ring maximum of reduced sulfur chemistry that may be dominant across the marginal Arctic environment. Sensitivity tests on this scenario include variation of cell sulfur composition and remineralization, routings/chemical time scales, and the physical dimension of water layers. An alternate possibility that peripheral additions are small cannot be excluded from the outcomes. It is concluded that seagoing dimethyl sulfide data are far too sparse at the present time to distinguish sulfur-ice production levels.

Citation: Elliott, S., C. Deal, G. Humphries, E. Hunke, N. Jeffery, M. Jin, M. Levasseur, and J. Stefels (2012), Pan-Arctic simulation of coupled nutrient-sulfur cycling due to sea ice biology: Preliminary results, *J. Geophys. Res.*, 117, G01016, doi:10.1029/2011JG001649.

1. Introduction

[2] The aerosol precursor molecule dimethyl sulfide is distributed inhomogeneously through waters of the marginal ice zone, but may act as a strong source of reduced sulfur to the Arctic atmosphere under many circumstances (DMS) [Ferek *et al.*, 1995; Lundén *et al.*, 2007]. Production distributions for polar DMS have not been clarified, and must include contributions from both ice algae and phytoplankton in the water column [Levasseur *et al.*, 1994; Matrai *et al.*,

2007]. We demonstrate here by attaching multielement geochemical cycles to a dynamic/thermodynamic sea ice model that epontic ecosystems could play a significant role, on a regional and seasonal basis. Essential nutrient and sulfur flow are coupled in our computations through a set of porous bottom layer kinetics simulations, with radiation inputs arriving from above through geographically distributed columns of snow and ice. Optimization tests on eco-dynamics of the major elements serve to reduce the number of broad biogeochemical scenarios, while variations in the model sulfur mechanism show that ice-derived peaks of greater than 10 nM are possible in remote areas. It becomes clear in the process, however, that measurement data are presently much too sparse and uncertain to permit a true quantification of error.

[3] Our development begins with individual descriptions of the program components. Some history and an overview of capabilities are provided for the dynamic sea ice model CICE [Hunke and Lipscomb, 2008; Hunke and Bitz, 2009]. Since the biogeochemistry involved becomes quite detailed whether regarding nutrients or the sulfur compounds,

¹Climate Ocean Sea Ice Modeling, Computational Sciences Division, Los Alamos National Laboratory, Los Alamos, New Mexico, USA.

²International Arctic Research Center, Institute of Marine Science, University of Alaska Fairbanks, Fairbanks, Alaska, USA.

³Institute of Arctic Biology, University of Alaska Fairbanks, Fairbanks, Alaska, USA.

⁴Department of Biology, Laval University, Quebec, Quebec, Canada.

⁵Laboratory of Plant Physiology, Center for Life Sciences, University of Groningen, Groningen, Netherlands.

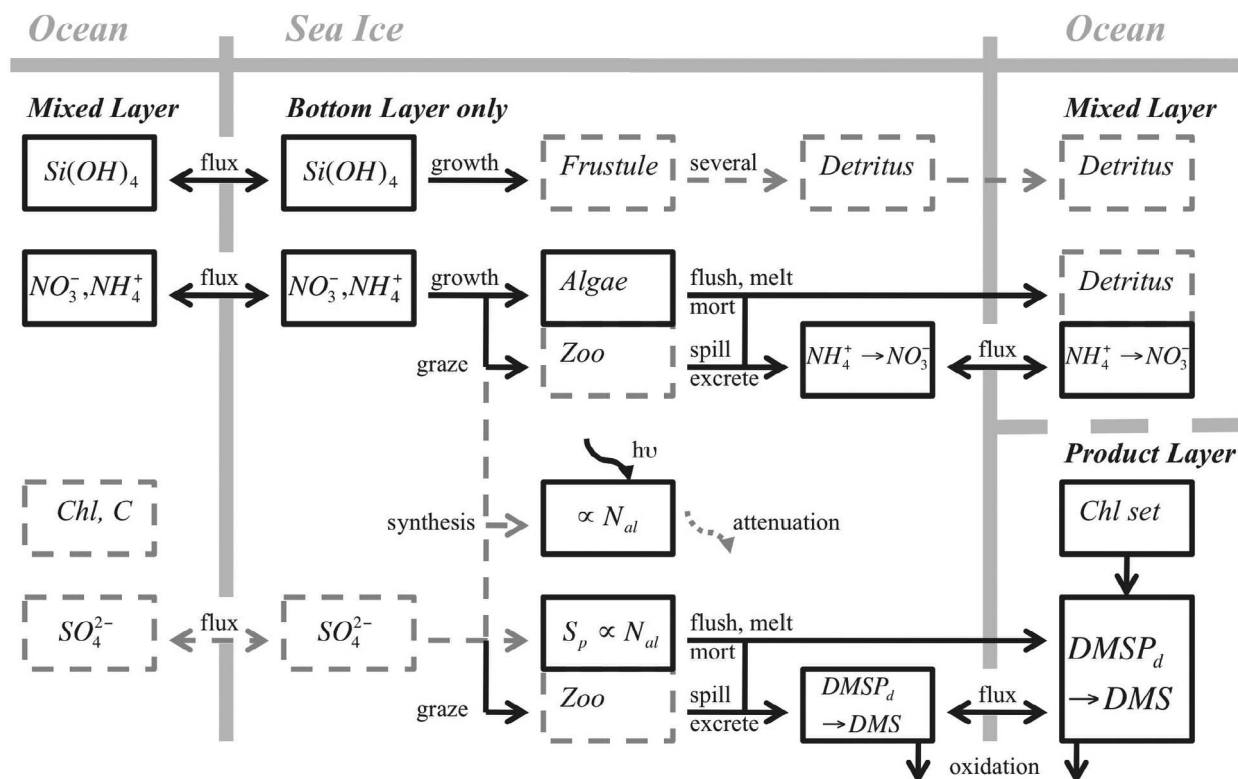


Figure 1. Schematic of coupled nutrient-reduced sulfur biogeochemistry attached to the CICE sea ice model in the present work. Solid rectangles and arrows indicate actual numerical tracers and the kinetic terms computed to interrelate them. Dashed quantities and arrows are dealt with implicitly or indirectly. Silicate uptake leads to formation by the pennate (ice) diatoms of frustules, one of the untracked materials. A portion of ablation from the biologically active layer is released directly into the water column. “Zoo” stands for zooplankton. Chlorophyll, carbon and particulate reduced sulfur concentrations are maintained proportional to ice algal nitrogen. Single trace element conversion reactions are shown internal to the multiple tracer boxes. Mixed and product layers are distinguished so that the latter can be thinned separately to reflect freshwater lensing.

background information is condensed into a set of appendices (Appendix A for parameters and Appendix B for equations). These are organized to emphasize our segregation of the reaction scheme into three layers or box models, all positioned just below CICE thickness categories. The numerical layers are assigned to represent nutrient injections from the water column source, processing in a well mixed ice volume and finally product buildup below the pack (Figure 1). The complete mechanism is subjected to merit function analysis, against selected bottom ice chlorophyll measurements (Table 1). We are careful to point out, however, that the procedure is nonglobal in its treatment of the parameter structure. Fine points of the epontic sulfur cycling are almost entirely unknown, and so we add them by drawing upon open water research along with some very recent ice core data [Stefels et al., 2007; Hellmer et al., 2008]. Variations are then imposed upon likely strong uncertainties, including average algal composition and loss rates during routing through or below the bottom layer (Table 2). Physical configuration of the model is adjusted systematically as well, through vertical dimensions of the

several chemical models which form the core of the approach (Appendices A and B).

[4] The trace element-ice simulations culminate in a set of distributions for dissolved dimethyl sulfide, a key agent of natural mass transfer to atmospheric particles [Charlson et al., 1987; Ferek et al., 1995; Lundén et al., 2007]. Annular features surrounding the Arctic and local concentrations up to tens of nanomolar are computed for heavily impacted surface waters. Even in a baseline case we show that the occasional well-studied ecosystem may be represented with fidelity and simultaneously, high concentrations are indicated on the periphery. But while one subset of sensitivity tests raises the maxima further, for others there is a potential dominance of external sources. DMS is among a small set of marine precursors influencing hygroscopicity of the remote aerosol, and hence also cloud droplet numbers [Andreae and Rosenfeld, 2008]. Effects on climate via the albedo are global in scope, but the importance is amplified at high latitudes [Zhou et al., 2001]. Although system simulations including ice biogeochemistry can now be used to bracket the uncertainties, we find that much more extensive

Table 1. A Subset of Collected Master Data Including Chlorophyll Measurements in Arctic Bottom Ice (mg/m²) and Dimethyl Sulfide Determined by Sparging in Subinterfacial Waters (nM)^a

	Okh	Lab	Ber	Chu	Can	Baf	Sva	Gyr	TPD
Jan									
Feb	40								
Mar	10–30	100		5			0.01		
Apr			(100)	15	1–10	10			
				1					
May				10–100	100–300	20		0.1–1	
Jun						10			
Jul							.03–0.3		
Aug				0.3			0.1	0.3–1	0.1–1
							1	1	0.3
Sep									0.1–1
									0.1
Chl	K97, M00	I90	D10, G99, G09	G97, G05, G09, U03	G99, G05, L94, M96, S97	L01	G97, G99, W07	G97, G05, G09, L99	G97, G99, LP96, L99
DMS				F95	F95		LP96	L99	LP96, L99

^aChlorophyll measurements are shown in italics and dimethyl sulfide values in bold. Entries are arranged chronologically downward but arrayed against a biogeography derived from Carmack and Wassman [2006] as adapted in our primary production work [Deal et al., 2011]. The ecozones are arranged roughly in latitudinal rank order. Most concentration values were first averaged then rounded to a final, single significant digit. Parentheticals are discussed only indirectly in the primary sources. Regional abbreviations are as follows: Okh, Sea of Okhotsk; Lab, Labrador Sea; Ber, Bering Sea; Chu, Chukchi Sea; Can, Canadian Archipelagic; Baf, Upper Baffin Bay; Sva, Svalbard and neighboring areas of the Greenland/Iceland/Norway Seas; Gyr, the Beaufort Gyre; and TPD, Transpolar Drift currents. Reference abbreviations are as follows: D10, Deal et al. [2011]; F95, Ferek et al. [1995]; G97, Gosselin et al. [1997]; G99, Gradinger [1999]; G05, Gradinger et al. [2005]; G09, Gradinger [2009]; I90, Irwin [1990]; K97, Kudoh et al. [1997]; LP96, Leck and Persson [1996]; L01, Lee et al. [2001]; L94, Levasseur et al. [1994]; L99, M. Levasseur, unpublished but cited in Sharma et al. [1999]; M96, Michel et al. [1996]; M00, Monfort et al. [2000]; S97, Suzuki et al. [1997]; U03, Uzuka [2003]; and W07, Werner et al. [2007].

measurements of reduced sulfur are needed both in the pack and in Arctic seawater.

2. Ice Dynamics and Biogeochemistry Connections

[5] Sea ice physics adopted here is that of the Los Alamos National Laboratory CICE model version 4 [Hunke and Lipscomb, 2008]. Coding descends directly from turn of the century viscous-plastic rheologies but with an elastic wave mechanism introduced that allows for explicit numerics and an accurate representation of the response to stress variations [Hunke and Dukowicz, 1997]. The method has ultimately been termed EVP for elastic-viscous-plastic, and it yields high fidelity results for the global pack field on short time-scales. The basis for incorporating waves is actually non-physical, but they render CICE especially well suited to the parallel supercomputing requirements inherent in modern

environmental simulations. Components interacting within the code include a thermodynamic subunit that computes local growth rates of snow and ice due to vertical conductive, radiative and turbulent fluxes [Bitz and Lipscomb, 1999]. Incremental remapping transport provides for the advection of areal concentration, ice volumes and other state variables [Lipscomb and Hunke, 2004]. A ridging parameterization is invoked to move masses of ice among thickness categories, based on energetic balance considerations and rates of strain [Lipscomb et al., 2007]. Over the last decade the CICE program has become standard within a major U.S. Earth System code, the CCSM or Community Climate System Model [Briegleb et al., 2004; Collins et al., 2006].

[6] In the present work, CICE is configured as a stand alone framework consistent with the latest, optimized Arctic coverage evolution experiments [Hunke, 2010]. The year 1992 was chosen as our focus, from a run extending across several decades of the late twentieth century. It is both

Table 2. A Selection From Among Sensitivity Calculations Conducted to Explore Uncertainties in the Sulfur Cycling^a

	Category					
Variation	Composition	Routings		Interchange	Timing	Physical
Specific	S/N Ratio	Graze (several)	Mortality (recycle)	Biomass return	S e-fold (several)	Box height (ice, below)
Layer(s)	Bottom	Bottom	Bottom	Bottom to product	Bottom and product	Bottom and product
Symbol	R _{S2N}	f _{ex}	f _{rem}	f _{rr}	τ	l ^{bot}
Baseline	0.03	0.5	1.0	0.1	10 d	0.03 m
Test	0.1	0.1	off	0.3	3 d	0.1 m
Δ DMS ^{pr}	Up ∞	Down 10s %	Down 100s %	Up 10s %	Down 3–5 \times , except center	Small
Location	Periphery	Blooms	Blooms	Melt	Periphery	All
Symbol		f _{sp}		f _{rr}	Exclude τ_{dis}	l ^{pr}
Baseline		0.5		0.1	10 d	10 m
Test		0.1		1.0	3 d	3 m
Δ DMS ^{pr}		Down 10s %	Up 100s %	Down 3–5 \times		Up ∞
Location		Blooms		Melt	All	Periphery

^aSymbols are defined in the parameter list in Table A1. Dimensionless quantities dominate toward the left side of the table, where emphasis is placed upon mole fractions and routings. Thereafter time and length units are indicated as appropriate. Product layer DMS concentration is the final gauge for major effects.

proximal to a period of intense sulfur measurement activity [e.g., *Levasseur et al.*, 1994; *Ferek et al.*, 1995], and typical of the Arctic situation prior to recent ice minimum years. All simulations were initialized in deep winter on the first of January and include full monthly variability over the four seasons. Results are taken from year one of a given run. Reseeding and overwintering mechanisms remain grossly understudied for the global ice biota and so they are not incorporated [*Arrigo and Thomas*, 2004; *Werner et al.*, 2007]. We propose to investigate interannual variability in more specialized studies.

[7] Contemporary Arctic ice biogeochemistry is confined largely to the bottom few centimeters of the column in any given location [*Levasseur et al.*, 1994; *Gradinger*, 1999; *Arrigo*, 2003; *Gradinger et al.*, 2005]. We therefore attached our geocycling scheme below the deepest CICE vertical division, in a series of kinetic box models of constant volume. The reactor layers represent respectively (1) input of the nutrients silicate, nitrate and ammonia from a data ocean, (2) nutrient and carbon cycling in the bottom ice itself, and finally (3) sulfur compounds ejected back into the water column. Mixed and product layer boxes are separated so that their thicknesses can be varied independently during the melt season, when thin brackish lenses may form just below the solid interface. Nutrients are consumed by the ice system and also replenished through remineralization. They can be restored to climatology through an adjustable time constant whose value is discussed in the optimization section. The several kinetic models carried as layers underneath CICE are computed on all thickness categories. Transport and geographic variation are thus experienced by the biology along with modulation of the radiation field by snow and ice. Tracer concentrations reported and plotted are grid cell averages, over all categories and percent coverages.

3. Biogeochemistry Model

[8] Multiple element geocycling added to CICE in the present work is shown schematically in Figure 1, which explicitly segregates the three reactor volumes employed. A geophysical context is displayed for each layer type, with respect to sea ice or underlying ocean waters. Note that there are no interactions in the current work with sediments, the continental shelf or with terrestrial processes. In the Pan-Arctic ocean to ice grid framework adopted, biogeochemistry actually rides underneath individual pack thicknesses. The mixed layer appears twice in the figure merely as a plotting convenience; in fact it is represented as a single entity within the numerics. Parameter settings and the equations represented by box-arrow relationships are summarized in two appendices. These refer primarily to a baseline case. Sensitivity testing is discussed in detail in section 6.

[9] Basin scale nutrient distribution patterns within the mixed layer were supplied to the model from available Arctic climatologies [*HAAO*, 2001; *Conkright et al.*, 2002]. The three main inorganic forms then equilibrate quickly into the bottom layer by mutual fluxing (nitrate, ammonium and silicate) [*Reeburgh*, 1984]. As sunlight becomes available at increasing latitudes, photon restrictions are lifted and the various fertilizers may be consumed from within the ice during photosynthesis [*Lavoie et al.*, 2005; *Jin et al.*, 2006]. Internal populations of the algae rise quickly as tracked

through their chlorophyll density, so that modeled uptake of the solutes soon outstrips backflow to the mixed layer. In most regions this leads to a fundamental flux limitation on the accumulation of biomass at the pack interface. The melt season initiates a bottom layer purge due to snow/surface drainage, and this excludes all solutes [*Vancoppenolle et al.*, 2010]. Organisms may be detached to varying degrees of effectiveness by the flush purge and also by continual ablation.

[10] Reduced sulfur chemistry is based on the assumption that the precursor compound DMSP_p (dimethyl sulfoniopropionate in particulate form) [*Stefels*, 2000] is synthesized and removed inside of ice algal cells in exact proportion to the main nitrogen currency. Rising S is later released by grazing and mortality processes into a decay sequence familiar from open waters [*Stefels et al.*, 2007]: DMSP_d (dissolved) is oxidized by free lysis enzymes plus bacteria to the volatile DMS (also dissolved, but this is traditionally unspecified). Time constants for the sequence are derived here mainly by applying a crude temperature slowdown relative to global averages [*Kiene and Bates*, 1990; *Leck and Persson*, 1996; *Stefels et al.*, 2007]. But they are entirely consistent with recent ice core studies with which one of us has been closely involved (J. Stefels, unpublished data, but see *Hellmer et al.* [2008] for a cruise summary). Once the decay series is established in simulated bottom ice, dissolved sulfur forms pass freely to and from the product layer.

[11] Polar DMS measurement campaigns are often also associated with chlorophyll determinations, and a steady background of below-ice biological activity is typically recorded [*Levasseur et al.*, 1994; *Leck and Persson*, 1996]. Usually between 0.1 and 1 mg/m³ of pigment are indicated and attributed to one of the nondiatom phytoplankton classes (e.g., flagellates; note that epontic algae are represented as pennate). In the model product layer, a reference chlorophyll level is thus maintained such that average cell disruption and oxidation time scales produce about a nanomolar of DMS. These values are forced externally, and function here mainly to provide a background in accord with the rare observations.

4. Data Sets

[12] We collected data for refinement of the model system by first seeking sulfur studies which also characterized the local biota, then extending to several icebreaker cruises. For ice bottom chlorophyll the values obtained in this manner are relatively numerous, but our survey is necessarily only partially complete. We obtain a Pan-Arctic band of values concentrated in bloom seasons and categorized biogeographically in Table 1. The data clearly show a well known trend toward tens of mg/m² at maximum along coastlines [*Gradinger*, 1999; *Arrigo*, 2003], plus a central ocean background which is orders of magnitude less concentrated but significant nonetheless [*Gradinger*, 1999]. Primary production measurements have been less extensive than those of biomass for the ice system [*Arrigo*, 2003], and they are not included in the validation process for the present work. Please see the companion piece from our group [*Deal et al.*, 2011] for a more complete discussion of biological production distributions.

[13] The sulfur situation contrasts starkly with that of the pigment data. Measurements are sparse to begin with, and

their interpretation is complicated by analytical chemistry problems which have only been understood in the last few years. There is a tendency for filtration to rupture algal cells, whether in open water or ice investigations. This inter-converts the critical quantities DMSP_p and a [Kiene and Slezak, 2006], so that only their sum is known accurately. From the most intense period of ice-sulfur study in the middle nineteen nineties [e.g., Levasseur et al., 1994; Ferek et al., 1995; Leck and Persson, 1996] many measurements must now be viewed merely as limits for these two species [Michaud et al., 2007]. The reported total DMS(P) data are more trustworthy [e.g., Uzuka, 2003], and DMS determinations conducted directly by gas sparging are still considered to be reliable. We insert the available purging data for under-ice DMS alongside those of the bottom layer chlorophyll, in the same table. After regional averaging procedures are applied as described in the caption, only a handful of points remain. In fact, we add to the available literature a set of results which have never before been published. The new data were obtained by one of us on a circum-continental study of the North American sulfur cycle [M. Levasseur in Sharma et al., 1999], and they are critical to the current process.

[14] Total measurements can indeed be located or partially reconstructed for the methylated sulfur compounds below an ice interface, or within the solid matrix ($\text{DMSP} + \text{DMS}$) [e.g., Levasseur et al., 1994; Lee et al., 2001; Uzuka, 2003]. But as a rule these quantities are also rare and poorly documented. Moreover, the artifact restrictions make all such results difficult to analyze for present purposes. Master lists of compiled sulfur chemistry information are available from the authors on request, but for the moment any data beyond the stripped DMS will be discussed explicitly only as the need arises. In general, our assessment is that the chlorophyll collection of Table 1 may be up to the task of adjusting major features of the overall ice biogeochemistry model, while sulfur measurements must for the moment serve mainly as a guide to future needs.

5. Optimization

[15] The model was configured at the outset to produce a minimum of biological activity, for example by reducing solute (flux) piston velocities to the brine exchange rate, and by ignoring reseeding [Wakatsuchi and Ono, 1983; Werner et al., 2007]. A stepwise selection procedure was then performed in order to establish a baseline [Gunst and Mason, 1980]. Stages in the calculation were organized chronologically to optimize model performance across the evolving seasons (Table 1). Parameters were prioritized for their importance to the system based mainly on expert judgment. They were then tuned to match the chlorophyll data, as judged by a minimum absolute error calculation performed relative to log transformed values [Zar, 1984].

[16] Startup concentrations of the algae were varied first and proved to be inconsequential, since exponential growth leads quickly to nutrient limitation. The mixed to bottom layer exchange velocity was then raised from the brine turnover rate upward, to account for boundary layer influences on the thickness of laminar entry barriers [Niedrauer and Martin, 1979; Wakatsuchi and Ono, 1983]. The interchange is treated in all our simulations as a Pan-Arctic

average, since our emphasis is on trace gas distributions. In the real ocean it will be faster coastally due to tides and regional currents [Cota and Horne, 1989; Gradinger, 1999; Lavoie et al., 2005]. The value 0.1 m/d has been judged maximal based on local, low dimensionality studies [Lavoie et al., 2005], and this was not exceeded. Basin scale nutrient patterns are supplied by the geochemical climatologies [HAAO, 2001; Conkright et al., 2002]. Initially they were allowed to drift per the concentration change equations. Reducing the restoration time, however, raised pigment distributions into agreement with data all the way up to the melt period. Ultimately the reset was lowered to zero days, so that model produced fluxes do not alter the oceanic distributions. Integrated vertical averaging of bottom layer radiation caused chlorophyll maxima to exceed the measured range in some low latitude seas [Arrigo, 2003], and so it was replaced by Beer's Law. We thus make the implicit assumption that photosynthesis shifts gradually toward lower portions of the bottom layer [Niedrauer and Martin, 1979; Smith et al., 1990]. This amounts to a self-shading approach [Arrigo et al., 1993].

[17] Rapid flushing of the nutrient and sulfur solutes is a given [Reeburgh, 1984; Jin et al., 2006], but removal of the algae themselves at the melt led to sharp biomass crashes and an inadequate autumn recovery (low populations late in the year). Although steep declines are observed in some studies [Jin et al., 2006], others suggest retention. The mix of scenarios over the polar regime is probably actually quite complex [Gosselin et al., 1997; Gradinger, 1999; Uzuka, 2003]. Organisms may seek refugia within the porous structure of ice and also rely on surface chemistry to maintain or improve their position [Krembs et al., 2000; Arrigo and Thomas, 2004]. We elected in the present work to treat algal removal mainly as a portion of and proportion to ablation, or equivalently as an adjustable time constant. Still the autumn rebound appeared to be slow and so we introduced a hard floor on biomass nitrogen levels (a lower limit that could not be bypassed). The intent was to simulate a combination of overwintering and the formation of cysts [Werner et al., 2007].

[18] Through these manipulations we were able to obtain an ice chlorophyll distribution agreeing with the Table 1 data to within a factor of two in most locations, and often much more closely. This simulation is defined henceforward as our baseline, and it is the one described most directly in the appendices. We recognize, however, that solutions to the stepwise optimization problem are non-unique and can be problematic at environmental scales [Gunst and Mason, 1980; Elliott, 2009]. The radiation and algal flushing treatments are particularly uncertain and could depend on the order of parameter refinement; for example, a rapid early purge might well preclude the need for internal shading. Such complexities were treated through independent tests conducted off line relative to the sulfur cycle.

6. Sensitivity Tests

[19] A series of parameter adjustment experiments was arranged in order to probe the wide variety of uncertainties in sulfur biogeochemistry pathways. A subset is listed with qualitative descriptors of the major outcomes in Table 2. Several broad testing categories are identified: algal

composition, routings and fractional exchange, time constants, and the dimensionality of the physical system itself were all manipulated systematically. It became apparent early on that concentration swings would regularly be strong for the major indicator, below-ice DMS. To simplify the situation, we adopted an informal strategy of alternating between parameter changes leading to increases and decrements.

[20] The first variation attempted was upon the Redfield-type sulfur to nitrogen ratio, for organisms dwelling inside the bottom layer. Ice is often portrayed as a stressful medium for algal growth [Levasseur *et al.*, 1994; Ferek *et al.*, 1995; Lee *et al.*, 2001; Stefels *et al.*, 2007]. But in fact this characterization is more apt for brine intensive upper level ecosystems, and these are somewhat disperse in the Arctic [Gradinger, 1999; Arrigo and Thomas, 2004]. Bottom ice conditions are favorable, since temperature and salinity are constrained to remain close to values for surface seawater. Nevertheless drainage and flushing will push epontic algae to osmotic extremes on occasion, and so we vary the sulfur content within constraints imposed by the few studies which can be readily interpreted to provide particulate mole ratios [e.g., Levasseur *et al.*, 1994; Uzuka, 2003]. This means roughly a factor of three in either direction. Dimethyl sulfide tends to track the composition of its source, but with dilutions superimposed from the central ocean background.

[21] The cascade of routings adopted to represent cell disruption is an especially ad hoc feature of the present model (Appendix B). Care has been taken to remain close to a straightforward mechanism pioneered by Arrigo *et al.* [1993], then propagated indirectly in related later works [e.g., Jin *et al.*, 2006]. Grazing is treated as a small, steady portion of the growth rate with constant fractions redistributed across the nitrogen cycle. Simplicity of the method is the primary recommendation, since it is doubtful that actual ice ecosystems exhibit such regularity. But alternate approaches are not readily available and marine biology simulators are typically developed with constant yields, whether at low or high latitudes [Archer *et al.*, 2004; Vallina *et al.*, 2008; Lavoie *et al.*, 2009]. Fractionations within the network were adjusted systematically in all pathways flowing from grazing and mortality. But effects proved to be most important for the mortality term. It is apportioned in the model only once, and further, co-varies with biomass rather than merely tracking primary production. The grazing channel by contrast becomes flux limited and is eventually outpaced; nutrient restrictions are felt immediately through Michaelis-Menten limitation functions.

[22] Pure time constants τ occur in both the bottom and product layer sulfur decay sequences, and also as a cell disruption rate in the under-ice reference flow. Conversion and oxidation reactions enfold complex processes involving mediation by a variety of bacteria and free enzymes [Kiene *et al.*, 2000; Stefels *et al.*, 2007]. Under-ice disruption really involves the same suite of channels illustrated in Figure 1. Since all these time scales were slowed intentionally relative to the global situation to attain a baseline, they were tested later by simultaneous downward perturbation. An interesting nonlinearity was quickly observed. In some regions concentrations of DMS fell by more than the rate proportionality. In section 7 we will attribute this effect to kinetic pathway shifts internal to the bottom layer.

Furthermore, it was realized at this point in the experiment that background injections should be treated independently from the overall water column metabolism. The magnitude of the reference source was thus fixed (product layer cell disruption maintained at 10 days). The central plateau of the DMS field became flexible under this combination of settings.

[23] Physical aspects of the code were varied over and above the biogeochemical tests just described. Flushing of the ice algae led to lengthy population dips reflected in strong losses of DMS in the summer. Return flow from either the purge or ablation could be adjusted to alter gas concentrations in the melt season. As detailed in section 5, integration of light fields over the whole bottom layer led to unrealistic bloom peaks. The sulfur content followed suit. Mixed, bottom and product layer vertical dimensions were each adjusted in turn. Key results from these height/volume alterations are outlined at the right side of Table 2. Since ice algae usually do not succeed in depleting nutrients before the break up [Gradinger, 1999; HAAO, 2001], thickness of the source pool proved inconsequential. The baseline run entails instantaneous restoration in any case. Perhaps surprisingly, depth of the bottom layer also turned out to be a neutral factor. Our interpretation is that under flux input limitation, all action centers on the interface whether it regards primary production or the eventual return of sulfur. Thinning of the product layer concentrated the outflow precisely as would be expected; the factors tested ranged up to an order of magnitude. Several lines of argument suggest that intermittent fresh water caps should form in the marginal zone [Gosselin *et al.*, 1990; Matrai *et al.*, 2008], but in view of the ice-breaker data at our disposal the baseline setting of ten meters seems reasonable (Appendix A) [Leck and Persson, 1996; Gosselin *et al.*, 1997].

7. Analysis

[24] Pan-Arctic plots generated from the nutrient element and sulfur simulations are organized as follows. The four central months of a baseline year are presented first, juxtaposing the columnar ice biomass and mixed layer dimethyl sulfide concentrations. Changes in the under-ice DMS are then analyzed for key test scenarios. In many cases reduced sulfur remains behind in surface waters of the mixed layer as the ice edge retreats, forming a residual field. This spreading effect is dealt with in this section as well. Sensitivity test results are presented only for the months of May and August, bounding the period of most intensive geochemical processing. All results are shown as monthly averages.

[25] In Figures 2 and 3 bottom algal chlorophyll and product layer DMS are shown side by side in May/June, then July/August. Poleward of the Arctic circle, sunlight only becomes available to support photosynthesis well past the equinox. May typically represents the peak in modeled ice biomass in more thoroughly studied regions, which are scattered along the Canadian Archipelago and North American coast [Cota and Horne, 1989; Levasseur *et al.*, 1994; Ferek *et al.*, 1995]. As one would expect based on our merit comparisons, peripheral chlorophyll ranges up to about one hundred mg/m², while values in the central ocean basin hover near unity. Local maxima are correlated mainly with mixed layer nutrient distributions, and anticorrelated with

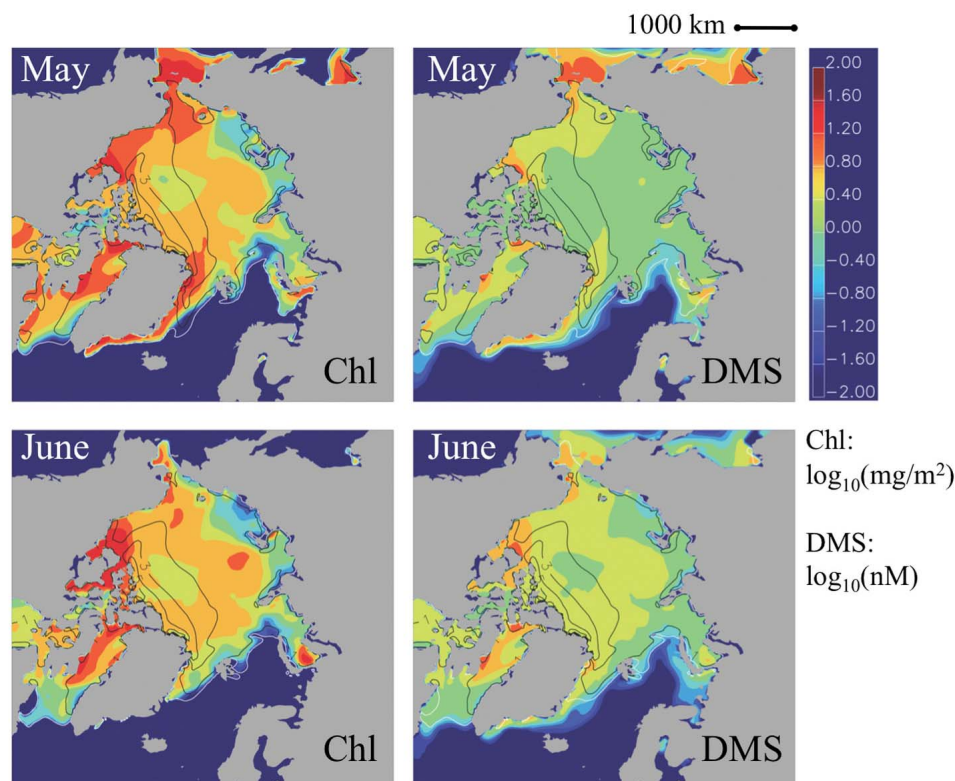


Figure 2. Baseline simulation of ice algal source organisms, (left) log₁₀ mg/m² chlorophyll, along with dimethyl sulfide injected into the ocean product layer, (right) log₁₀ nM, in May and June of 1992. Ice edges are defined by the 15% ice concentration contour (white), and thicknesses are superimposed in meters (black).

snow cover [Lavoie *et al.*, 2005; Jin *et al.*, 2006]. The bloom annulus tends to roll inward toward the pole as a function of time in simulations such as these, following integrated radiation penetration.

[26] DMS distributions in our baseline mechanism are closely related to the modeled primary production and/or biomass, but are not strictly proportional to them. A term-by-term breakdown of the equations in Appendix B demonstrates that during the early period of rapid chlorophyll accumulation, release by the grazing fraction is dominant. The in-ice mortality channel soon takes precedence, however, and this mitigates to some extent the difficulties associated with a constant, steady apportionment (see section 6 and Appendix B). Both pathways inject DMSP_d into the bottom few centimeters of the solid matrix, with rapid flux removal into the mixed layer followed by conversion to DMS. Melting augmentation of below-ice buildup occurs early on at low latitudes, via partial sloughing of cells and then their (implicit) disruption below the ice. Maxima displayed in Figures 2 and 3 can be attributed to the conjunction of these sources and reach up to 30 nM.

[27] Peaks in the mixed layer sulfur distribution are critical features of the simulation, because they may directly augment flow to the atmosphere from margins or leads [Ferek *et al.*, 1995; Lundén *et al.*, 2007]. It can be shown by applying analytical reaction/transport calculations to the seasonal permeability [Vancoppenolle *et al.*, 2010] that direct escape through the solid matrix will be rare except for thin

or warming (porous) systems. For most central basin and land-fast pack ice, solute movement is suppressed by brine channel closure during winter, and then by downward flushing during the melt [Jin *et al.*, 2006]. Leads, however, form continually along the periphery and appear deep in the ocean center during summer. DMS produced under such a network of openings will rapidly be available for sea-air transfer [Ferek *et al.*, 1995; Matrai *et al.*, 2007].

[28] A 15% ice concentration contour is indicative of the pack edge [e.g., Hunke and Bitz, 2009], and this is represented explicitly on all our plots. Algal production will continue for tens of kilometers on either side of this semi-arbitrary threshold, both in the model and reality. On the seaward side, horizontal transfer to open water becomes especially fast. Sulfur interconversion via lyase enzymes and the oxidation each require ten days in our baseline model (see Appendices A and B), so that compounds sourced from the bottom layer can be transported for weeks in open water. Note that the field of ice-derived DMS often lingers well beyond that of chlorophyll in the figures. No attempt is made here to simulate the dynamics of sea-air transfer, but the time constant for the process is roughly days to several weeks so that it will be competitive with oxidation [Stefels *et al.*, 2007; Elliott, 2009].

[29] It is clear from the sequence of images in Figures 2 and 3 that our optimized mechanism produces volatile sulfur concentrations in excess of several nanomolar in many locations. The distribution takes the form of a punctuated

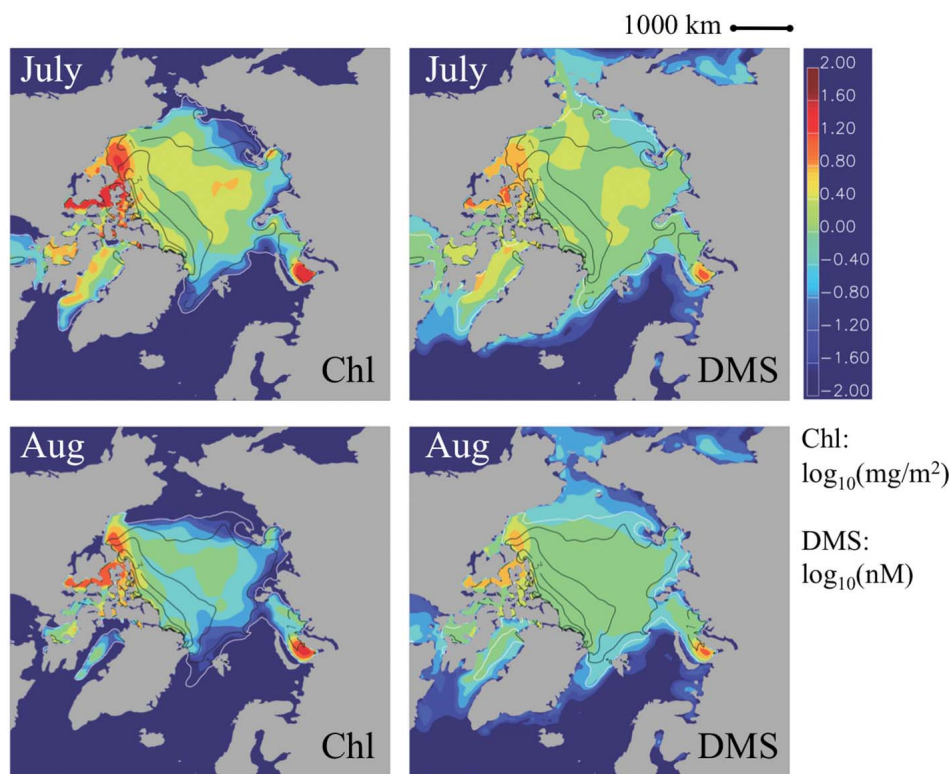


Figure 3. Baseline simulation of ice algal source organisms, (left) \log_{10} mg/m^2 chlorophyll, along with dimethyl sulfide injected into the ocean product layer, (right) \log_{10} nM, in July and August of 1992. Ice edges are defined by the 15% ice concentration contour (white), and thicknesses are superimposed in meters (black).

band of activity ringing the ice zone and also extending poleward for some distance. On the logarithmic color bar, yellow tones and brighter correspond roughly with concentrations comparable to those measured in open northern waters (3 nM is a reasonable reference point) [Leck and Persson, 1996; Kettle and Andreae, 2000; Matrai et al., 2007]. Thus one particularly compelling scenario which emerges from our exercise is the following: an imperfect polar cap only partially contains strong and somewhat unexpected sources of a critical, climate-influencing trace gas. This result is consistent with arguments from the seminal work of Levasseur et al. [1994] and follow-ons [Ferek et al., 1995; Sharma et al., 1999; Lee et al., 2001], which discuss the concept of polar pulses of reduced sulfur to the troposphere.

[30] The DMS database is so sparse, however, that it is difficult to achieve any degree of validation. Early sparging samples taken below the ice off coastal Alaska and Canada in springtime suggest concentrations of between 1 and 10 nM [Ferek et al., 1995]. Icebreaker cruises give convincing evidence for a steady background of 0.1 to several nM beneath the central pack, extending along the prime meridian and across the pole [Leck and Persson, 1996; Sharma et al., 1999]. Unpublished data associated with the latter reference demonstrate a slight relative excess in the solid bottom layer. Results offered in Figures 2 and 3 can be viewed as conforming with all the above. But the constraints are very weak and a large portion of the agreement is guaranteed by our product layer reference flow.

[31] The most instructive results from the sulfur test series introduced in Table 2 are illustrated in Figures 4 and 5, for early and late periods of high northern geochemical activity (May and August). Shown clockwise from top left are an increased bottom layer sulfur to nitrogen ratio for the ice algae (Figures 4a and 5a), lowered remineralization fraction (relative to the mortality term) (Figures 4b and 5b), strongly elevated melt return to a mixed layer lying just below the ice interface (Figures 4c and 5c), and reductions to the chemistry time scales (Figures 4d and 5d). Details of the variation procedures are provided in paragraphs just below, with reference to the parameters in Appendix A and the equations in Appendix B. In Figures 4 and 5 it is apparent that a basic ring structure is retained for the maxima, but it is modulated severely around the pole acting as a central axis.

[32] Strong upward sensitivity was demonstrated by the ice-layer Redfield ratio (4 and 5 upper left). A baseline value 0.03 by moles was altered to the round figure one tenth, still well within the measurement range for composition [Levasseur et al., 1994; Uzuka, 2003; Stefels et al., 2007]. Response of the DMS concentration pattern is simple and almost directly proportional, but nonlinearities rapidly become the rule rather than the exception. Multiple adjustments were imposed on the grazing branches, to explore variations in the downward direction. Initially we were surprised by weakness of the collective influences, and in fact this led to recognition of the dominance by mortality. Since the time constant for senescence is relatively slow, it was not a priori expected to compete. A series of

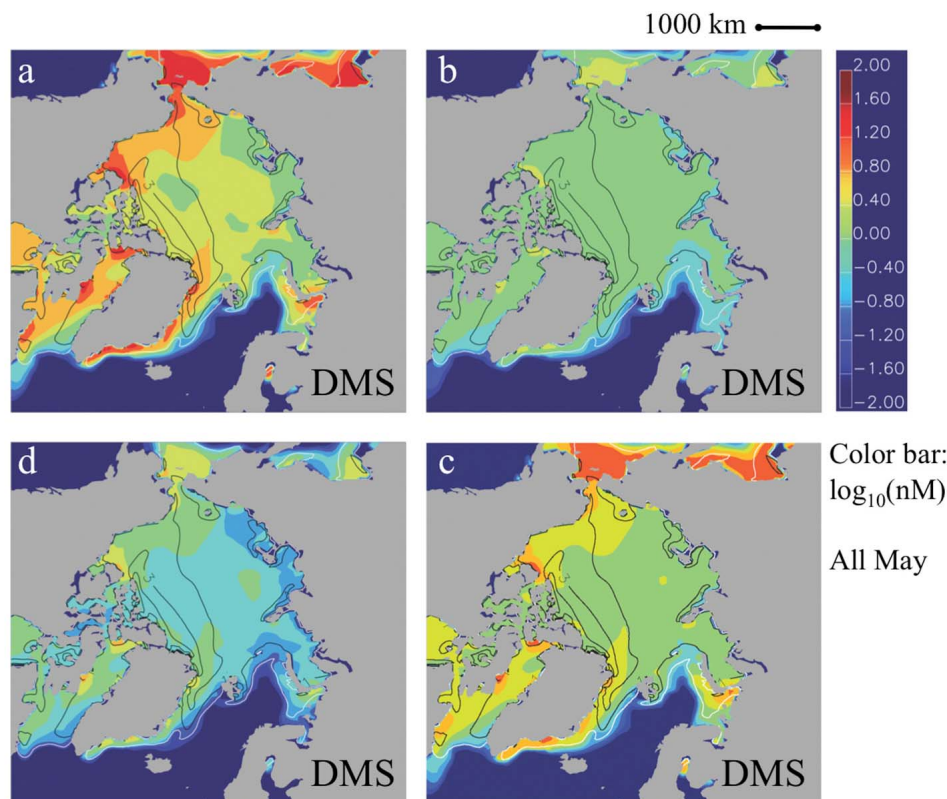


Figure 4. Product layer dimethyl sulfide distributions from four sensitivity tests conducted in May 1992. Clockwise from upper left: (a) Bottom layer sulfur to nitrogen ratio raised to one tenth; (b) remineralization fraction zeroed for the mortality channel; (c) melt fraction return of methylated sulfur raised to unity; (d) most chemical lifetimes shortened to 3 days. Units and ice property indicators are as defined in Figures 2 and 3.

simulations was ultimately conducted in which the mortality remineralization fraction was lowered systematically. In order to generate Figures 4b and 5b, apportionment of the returning ecodynamic nitrogen flow was zeroed entirely. Resulting changes are strongest relative to the bloom peaks of the first two images. Note for instance the strong losses of dimethyl sulfide in the Seas of Okhotsk and Bering, and also along the Atlantic coast of Greenland.

[33] Changes in the appendix network of fractional routings were intended mainly to perturb the sulfur cycle, but since mass is partially conserved across algal soft parts there were reverberations into the nitrogen system as well. The effects were most noticeable for the remineralization channel, but net degradation to the model optimum was always slight. Chlorophyll levels and mean absolute error (logarithmic) never differed by more than a few percent locally from the baseline. Where the mechanism permitted through inclusion of sulfur-only switches (2S in the parameters of Table A1), we verified that the several elemental cycles could in fact be decoupled completely. Baseline chlorophyll distributions were fully restorable. Taken together, these runs indicate that recycling is a minor factor in the current model. We do not claim, however, that this will universally be the case [Arrigo *et al.*, 1993; Gradinger *et al.*, 2005]. Further experimentation on the major element routings should be encouraged and supported.

[34] Continuing through the same figures in a clockwise manner, semi-arbitrary melt reintroductions were bolstered to produce Figures 4c and 5c. The baseline fractionation for this pathway was reset from the original round value of 10 to 30 and then 100 percent. Only the latter result is shown. Here the discrepancies are highly nonlinear, because they are diluted by either the mortality path or the mixed layer background depending on distance from the coast. In May noticeable shifts are apparent in the enclosed Pacific seas toward the top of the image, where ice loss begins earliest in the year. The behavior off Labrador is similar. In many areas, however, the effects are not easy to identify and serve to underscore the relative importance of the recycling and background channels.

[35] Various combinations and permutations were simulated for the multiple, independent conversion time constants. Mainly the direction of these experiments could be readily anticipated: for a given input, faster removal merely reduced the sulfur product load. But several complexities emerged which are less than obvious. A standard reduction from 10 to 3 days was selected for most of the studies and parameters. In one particular run for which all lifetimes were reduced together (cell disruption plus DMSP conversion and DMS oxidation in both layers), the tendency for concentration buffering in the central Arctic was preserved. Production and removal changes completely balanced one

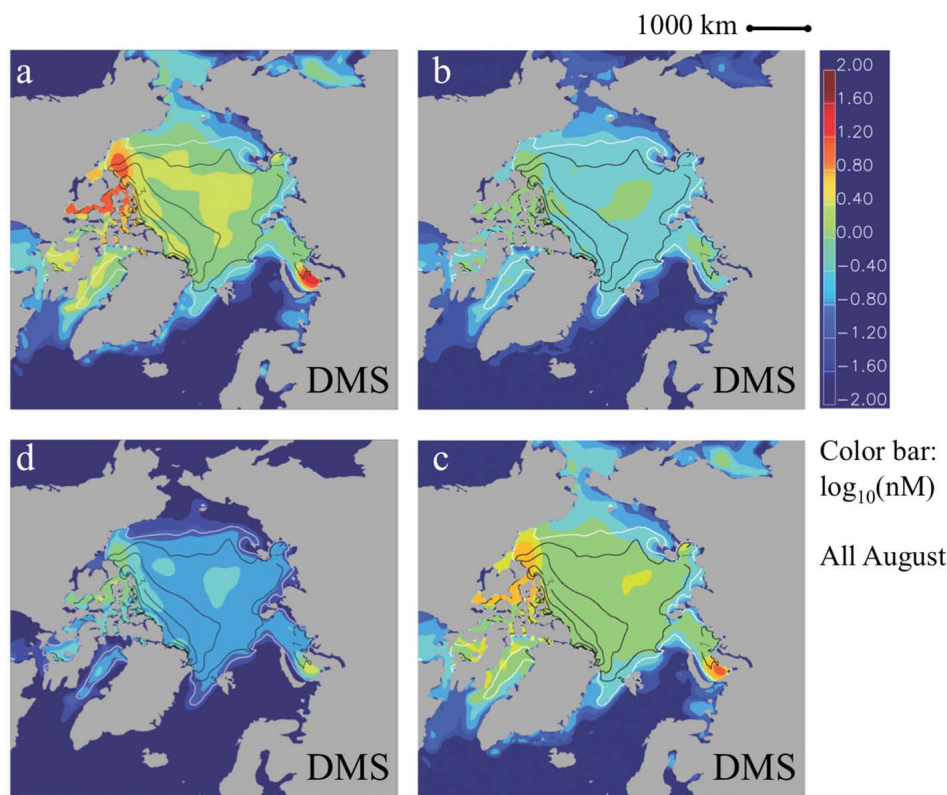


Figure 5. Product layer dimethyl sulfide distributions from four sensitivity tests conducted in August 1992. Clockwise from upper left: (a) Bottom layer sulfur to nitrogen ratio raised to one tenth; (b) remineralization fraction zeroed for the mortality channel; (c) melt fraction return of methylated sulfur raised to unity; (d) most chemical lifetimes shortened to 3 days. Units and ice property indicators are as defined in Figures 2 and 3.

another for the product layer in this case. From then on, the mixed layer disruption constant was restored to 10 days and maintained at this level. In the final set of images results are shown for speedups to 3 days excluding the below ice release (increases to the rate constant (Figures 4d and 5d)). The level, central basin background of 1 nM is lost and elsewhere, actual reductions to the mixed layer trace gas concentration exceed the factor $10/3 = 3.3$. They may be as large as a factor of four or five locally. It becomes clear that the relationship between outbound flux and conversion/oxidation is modulated within the bottom layer. Changes from the pure chemistry are then superimposed in the sub-ice realm.

[36] Results from these tests and analyses can be interpreted in bulk since uncertainties in the system are so widespread. Across our final two figures and assessed against the baseline, volatile sulfur rises from roughly ten to tens of nanomolar in many places, or else is reduced to near absence in some instances. Maxima cluster in adjacent seas and also the coastal archipelagos (e.g., Canadian, Novaya Zemlya, Eastern Greenland fjordlands). Lows hover around the pole. But the essential sparge-type measurements for under-ice dimethyl sulfide are only available in a handful of intermediate areas, and these do not happen to correspond with strong variability. It is thus difficult to eliminate any of the rather extreme possibilities highlighted by the model for the volatile sulfur distribution. Plus it must be recalled, our

driver (major element) optimization strategy is nonglobal in the parametric sense and open to question in its own right.

8. Summary and Discussion

[37] Numerical models are now available for representation of both the physics and biogeochemistry of global sea ice, and they may be applied together to simulate the behavior of climate-active tracers in marginal waters. We combine several of our own codes here to estimate the contribution from bottom ice layers to Arctic seawater dimethyl sulfide. Calculations extend across the central ocean and into neighboring seas, for a typical climatological year prior to the turn of the century. DMS is produced in the lower few centimeters of the solid matrix by ice algae [Levasseur *et al.*, 1994; Uzuka, 2003], whose growth is in turn supported by upward nutrient fluxes from the water column [Lavoie *et al.*, 2005; Jin *et al.*, 2006]. Key quantities adopted into our mechanism from the physical CICE code are snow and ice thickness, which determine light penetration [Hunke and Lipscomb, 2008; Hunke and Bitz, 2009]. Positioning of the pack over marine nitrate and silicate fields is also critical [HAAO, 2001; Conkright *et al.*, 2002].

[38] Biogeochemical reaction schemes are carried as a set of interlocking kinetic box models, configured as layers representing (1) nutrient injections from beneath the CICE grid, (2) processing of the biolimiting elements and sulfur in

porous bottom materials, and (3) reinjection of methylated precursors plus DMS into freshened waters adjacent to the interface. Integrated ice chlorophyll data are relatively plentiful across the Arctic environment [Arrigo, 2003]. A selected subset is applied here in merit function mode, to down-select for basic nutrient and biomass relations. In the model derived, critical levers are the interfacial transfer velocity, internal shading and treatment of algal removal. Our DMS production sequence is patterned after broad features of the global marine sulfur metabolism [Stefels, 2000; Stefels et al., 2007; Elliott, 2009], supplemented with time constants from recent Antarctic sea ice core studies. Baseline distributions obtained below the pack do not contradict measurements, but reliable data are only available from a few locations [Ferek et al., 1995; Leck and Persson, 1996]. In many peripheral Arctic ecosystems, the potential exists for volatile sulfur maxima to exceed 10 nM given ice inputs alone. Marginal cruise data are likewise in accord but non-discriminating [Leck and Persson, 1996; Matrai et al., 2007]. Sensitivity tests conducted on organism composition, reaction pathways within and/or below the ice, vertical layer dimensions and other model features leave these general conclusions in place. But they also open the possibility that contributions on the periphery of the ice domain are much less significant.

[39] Our chlorophyll comparisons are tailored to the requirements of a sulfur study in several crucial ways. Multiple data sets are cited, but the majority are linked with DMS campaigns so that a complete survey is not achieved; independent measurements are available which remain unexploited here. The baseline mechanism was refined in a stepwise procedure which is nonglobal in its sampling of the parameter space. A more thorough strategy could well yield areas of enhancement. It might be possible, for example, to elucidate the geographic distribution of ice-ocean boundary layer flux controls, or the roles of flushing and melt retention in determining bloom strength [Gradinger, 1999, 2009; Lavoie et al., 2005; Jin et al., 2006]. In order to affect our more important results, however, chlorophyll additions would have to be focused in a few remote hot spots. Sparsity is the current watchword, and this is particularly true outside familiar research zones of the U.S. and Canada. In a companion paper from our group [Deal et al., 2011], an analog model system is applied to the Pan-Arctic primary production problem. Simulated pigment distributions are quite similar, suggesting that ensembles might be used to investigate the plasticity of regional biogeochemical fields.

[40] Although much can be learned from such numerical exercises, the strongest impression we are left with regarding the ice sulfur cycle is one of pervasive uncertainty. It abounds in all aspects of the epontic geocycling, but the difficulties are amplified zooming on a specific tracer. A prioritized list for improvements in an ice domain DMS model would have to encompass all the following parameterizations: water-ice solute transfer, absorption of radiation, bottom layer purging, melt release of organisms or detritus, and the abundance of artificial routings which interject themselves. Our analysis suggests that these issues will be relevant across the spectrum of elements and compounds now drawing polar research attention. It may soon be necessary to consider ice column chemical interactions for volatile halogens, trace metals, their inorganic and organic ligands, and new crystalline phases [Lannuzel et al., 2007; Saiz-Lopez et al., 2007; Rysgaard

et al., 2009]. Detailed processes entering into ice biogeochemistry models will resemble the above in many cases, with perhaps an increased emphasis on resolution.

[41] Networks of ecodynamic flow are particularly intricate in the sulfur case [Kiene et al., 2000; Stefels, 2000; Stefels et al., 2007; Vallina et al., 2008], and our ice simulations underscore this point effectively. Panning across and down the Figure 1 schematic, it is evident that a highly interactive web drives the trace gas response, distributed across several phases. It may be that the only path which is well understood at this point is the one followed by silicon [Lavoie et al., 2005, 2009]. The percentage-level grazing fractionation seems to be real, but intensity of the biomass diversion may be either larger or smaller than we have specified, and it may be vertically differential [Gradinger et al., 2005]. Recycling could be more important than anticipated here [Arrigo et al., 1993; Lavoie et al., 2005; Jin et al., 2006]; the reader will note that reactions within the bottom layer by and large follow a single metabolic direction. Unresolved questions are the rule rather than the exception in the present work. It is difficult to escape the conclusion that this particular discipline is only in its infancy. Possible outcomes could be narrowed substantially through renewed laboratory and field work; for example, see *Levasseur et al.* [1994] and *Krembs et al.* [2000] or the isotope studies mentioned by *Hellmer et al.* [2008]. But it remains an open question whether such investigations can keep pace over the next few decades with Arctic environmental change.

[42] Under these circumstances a preferred strategy for the application of systems modeling is to bracket uncertainty. The existing ensemble of global carbon cycle codes is already viewed in this manner [Meehl et al., 2007], and a growing collection of sulfur analogs may soon follow. Intercomparisons are now available for the full set of contemporary open water DMS simulations [Le Clainche et al., 2010]. As international groups extend their approaches to encompass ice algae and as coupled ocean-pack models are placed in a global change context, it should be possible to begin the quantification process. Specifically the plan for our team is to work toward ice, aerosol, cloud interactions within the U.S. Community Climate System Model (CCSM). Ultimately we hope to investigate the uncertainties in biogeochemistry-to-brightness relations, for future polar climate scenarios.

Appendix A: Parameters

[43] Values incorporated into the baseline simulation are given in the center of Table A1 as a set of examples. The reader will note that heavy reliance has been placed on the coastal (Chukchi) silicon/nitrogen formulation of *Jin et al.* [2006], which also constitutes the core of our primary production study [Deal et al., 2011]. Alternate frameworks can and will be tested with sulfur at a later date.

Appendix B: Equations

[44] Time rates of change for the biogeochemical quantities under consideration are given in the following equation list, with individual terms defined further below. Superscripts “ml, bot, pr” signify the mixed, bottom and product

Table A1. Parameters of Our Multielement Ice Biogeochemistry Model^a

<i>Dimensions</i>				
Quantity	Symbol	Base	Units	References and Comments
Mixed layer thickness	l^{ml}	30	m	S95, G97
Bottom layer thickness	l^{bot}	0.03	m	NM79, R84, L05, J06
Product layer thickness	l^{pr}	10	m	G90, S95
<i>Mixed Layer Nutrients $\text{Si}(\text{OH})_4$, NO_3^-, NH_4^+</i>				
Quantity	Symbol	Base	Units	References and Comments
Exchange velocities	$v_{\text{flux, flush}}$	0.1	m/d	Optimized here plus L05, J06
Nitrification time scale	τ_{nit}	66	d	J06
<i>Bottom Layer Si, N, C, Chl</i>				
Quantity	Symbol	Base	Units	References and Comments
Chlorophyll attenuation	a_{chl}	0.03	1/(mg/m ³)	L05
Normalized P versus I	α/P_{max}	0.8	1/W/m ²	J06
Light inhibition	β/P_{max}	0.02	1/W/m ²	J06
Growth preexponent	g_{pre}	1.5	1/d	J06
Growth T dependence	g_{exp}	0.06	1/C	J06
Nutrient half saturations	K_{nut}	4,1,1	mmol/m ³	J06, nut = $\text{Si}(\text{OH})_4$, NO_3^- , NH_4^+
Ammonia inhibition	χ	1.5	1/mmol/m ³	J06
Fraction respired	f_{res}	0.05	nondim	J06
Fraction grazed	f_{gra}	0.1	nondim	A93, L05, added to source sulfur
Graze assimilated, spilled	$f_{\text{as, sp}}$	0.5, 0.5	nondim	Central values for base case
Assimilation excreted	f_{ex}	0.5	nondim	Central value for base case
Mortality preexponent	m_{pre}	0.02	1/d	J06
Mortality T dependence	m_{exp}	0.03	1/C	J06
Mortality remineralized	f_{rem}	1	nondim	Added for sulfur testing
Nitrification time scale	τ_{nit}	66	d	J06
Exchange velocities	$v_{\text{flux, flush}}$	0.1	m/d	Optimized here plus L05, J06
Algae flushed	f_{fl}	0	nondim	Optimized here plus G97, G99
Algae ablated	f_{me}	0.1	nondim	Optimized here plus G97, G99
Ice algal composition	R_{X2N}	9, 1.5	mole/mole	CH89, S90, L05, J06, X = C, Si
Ice algal pigments	R_{Chl2N}	3	g/mole	CH89, S90, L05, J06
<i>Bottom Layer Sulfur</i>				
Quantity	Symbol	Base	Units	References and Comments
Ice algal composition	R_{S2N}	0.03	mole/mole	L94, U03
Excretion to sulfur	f_{ex2S}	1	nondim	Initially assumed efficient
Mortality to sulfur	f_{mo2S}	1	nondim	Initially assumed efficient
Conversion time scale	τ_{con}	10	d	>~one week
Conversion yield	Y_{con}	1	nondim	Initially set to unity
Oxidation time scale	τ_{ox}	10	d	>~one week
<i>Product Layer General</i>				
Quantity	Symbol	Base	Units	References and Comments
Chlorophyll below ice	Chl^{pr}	0.1	mg/m ³	LP96, G97, fixed
Algal composition	R_{C2N}	7	mole/mole	Nondiatoms, so no Si L94
Algal pigments	R_{Chl2N}	3	g/mole	L94, G97
Cell disruption time	τ_{dis}	10	d	>~one week
<i>Product Layer Sulfur</i>				
Quantity	Symbol	Base	Units	References and Comments
Algal composition	R_{S2N}	0.03	mole/mole	L94, U03
Fraction melt return	f_{tr}	0.1	nondim	Rapid sinking in L09
Conversion time scale	τ_{con}	10	d	>~one week
Conversion yield	Y_{con}	1	nondim	Initially set to unity
Oxidation time scale	τ_{ox}	10	d	>~one week

^aReference abbreviations are as follows: A93, Arrigo *et al.* [1993]; CH89, Cota and Horne [1989]; G90, Gosselin *et al.* [1990]; G97, Gosselin *et al.* [1997]; G99, Gradinger [1999]; J06, Jin *et al.* [2006]; L05, Lavoie *et al.* [2005]; L09, Lavoie *et al.* [2009]; LP96, Leck and Persson [1996]; L94, Levasseur *et al.* [1994]; NM79, Niedrauer and Martin [1979]; R84, Reeburgh [1984]; S95, Schlosser *et al.* [1995]; S90, Smith *et al.* [1990]; and U03, Uzuka [2003].

numerical layers. Subscripts refer mainly to specific processes or the materials cycled by them. An exception occurs in the composition ratios, where for example “S2N” indicates a molar sulfur to nitrogen ratio.

$$\frac{dSi(OH)_4^{ml}}{dt} = \frac{F_{Si(OH)_4}}{l^{ml}} \quad (B1)$$

$$\frac{dNO_3^{-ml}}{dt} = k_{nit}NH_4^{+ml} + \frac{F_{NO_3^-}}{l^{ml}} \quad (B2)$$

$$\frac{dNH_4^{+ml}}{dt} = -k_{nit}NH_4^{+ml} + \frac{F_{NH_4^+}}{l^{ml}} \quad (B3)$$

$$\frac{dSi(OH)_4^{bot}}{dt} = -U_{Si(OH)_4}^{bot} - \frac{F_{Si(OH)_4}}{l^{bot}} \quad (B4)$$

$$\frac{dNO_3^{-bot}}{dt} = k_{nit}NH_4^{+bot} - U_{NO_3^-}^{bot} - \frac{F_{NO_3^-}}{l^{bot}} \quad (B5)$$

$$\begin{aligned} \frac{dNH_4^{+bot}}{dt} = & (f_{res} + f_{ex}f_{as}f_{gra})G^{bot} + f_{rem}M^{bot} - k_{nit}NH_4^{+bot} \\ & - U_{NH_4^+}^{bot} - \frac{F_{NH_4^+}}{l^{bot}} \end{aligned} \quad (B6)$$

$$\frac{dN_{al}^{bot}}{dt} = (1 - f_{gra} - f_{res})G^{bot} - M^{bot} - \frac{F_{al}}{l^{bot}} \quad (B7)$$

$$\frac{dC(Chl, S)_{al}^{bot}}{dt} = R_{X2N}^{bot} \frac{dN_{al}^{bot}}{dt}, \quad \frac{dS_{al}^{bot}}{dt} = 0, \quad \frac{dS_{al}^{bot}}{dt} = \frac{dDMSP_p^{bot}}{dt} \quad (B8)$$

$$\begin{aligned} \frac{dDMSP_d^{bot}}{dt} = & R_{S2N}^{bot} \left((f_{sp} + f_{ex2S}f_{ex}f_{as})f_{gra}G^{bot} + f_{mo2S}f_{rem}M^{bot} \right) \\ & - k_{con}DMSP_d^{bot} - \frac{F_{DMSP_d}}{l^{bot}} \end{aligned} \quad (B9)$$

$$\frac{dDMSP^{bot}}{dt} = Y_{con}k_{con}DMSP_d^{bot} - k_{ox}DMSP^{bot} - \frac{F_{DMS}}{l^{bot}} \quad (B10)$$

$$\begin{aligned} \frac{dN(C, Chl, S)_{al}^{pr}}{dt} = & 0, \quad Chl_{al}^{pr} = empirical, \\ S_{al}^{pr} = & DMSP_p^{pr} = \left(\frac{R_{S2N}^{pr}}{R_{Chl2N}^{pr}} \right) Chl_{al}^{pr} \end{aligned} \quad (B11)$$

$$\frac{dDMSP_d^{pr}}{dt} = R_{S2N}^{bot} f_{rr} \left(\frac{F_{al}}{l^{pr}} \right) + k_{dis}DMSP_p^{pr} - k_{con}DMSP_d^{pr} + \frac{F_{DMSP_d}}{l^{pr}} \quad (B12)$$

$$\frac{dDMS^{pr}}{dt} = Y_{con}k_{con}DMSP_d^{pr} - k_{ox}DMS^{pr} + \frac{F_{DMS}}{l^{pr}} \quad (B13)$$

Beginning with the differentials for pure elements, “al” points directly to the ice algae. Throughout the above, “k” are pseudo-first-order rate constants obtained as reciprocals of corresponding time scales from Table A1. Note that the term for nitrification $k_{nit}NH_4^+$ is similar in the source and ice processing zones.

[45] Chemical and biological tracers can be placed into vectors T specific to each of the three layers supporting ice domain geocycling, for purposes of generalization. Their concentrations are then

$$T^{ml} = Si(OH)_4, NO_3^-, NH_4^+ \quad (B14)$$

$$T^{bot} = Si(OH)_4, NO_3^-, NH_4^+, Si_{al}, N(C, Chl, S)_{al}, DMSP_d, DMS \quad (B15)$$

$$T^{pr} = N(C, Chl, S)_{al}, DMSP_d, DMS \quad (B16)$$

$$S_{al} = DMSP_p \quad (B17)$$

These are carried in units of millimole per m^3 , excepting mg/m^3 in the case of chlorophyll. The first few composite terms in the equation list may now be expressed as

$$F_{sol} = v_{flux}(T_{sol}^{bot} - T_{sol}^{ml}) \text{ or } v_{flush}T_{sol}^{bot} \quad (B18)$$

$$U_{nut}^{bot} = R_{X2N}^{bot} f_{nut} G^{bot} \quad (B19)$$

$$G^{bot} = L_{total} g_{pre} e^{g_{exp} C^v} N_{al}^{bot} \quad (B20)$$

in which F is a flux, U is an inorganic uptake, and G is overall growth tracked in the fundamental nitrogen currency. Subscripts “sol” and “nut” specify all solutes or else just the inorganic nutrients. Total growth limitation L_{total} accounts for contributions related to radiation, individual source materials, and also the required elements. To calculate the subterms, we draw on the biomass distribution for attenuation, then on concentrations in order to build saturation curves and apportionments.

$$I_{avg} = I_{lower\ bound} = I_o e^{-a_{Chl} Chl^{bot\ bot}} \quad (B21)$$

$$L_{rad} = \left(1 - e^{-(\alpha/P_{max})I_{avg}} \right) e^{-(\beta/P_{max})I_{avg}} \quad (B22)$$

$$L_{nut} = (T_{nut}^{bot} / (T_{nut}^{bot} + K_{nut})) e^{-\chi_{NH_4^+}} \quad (B23)$$

$$L_{element} = \sum_{nut} L_{nut} \quad (B24)$$

$$f_{NO_3^-, NH_4^+} = \frac{L_{nut}}{L_{element}}, \quad f_{Si(OH)_4} = 1 \quad (B25)$$

$$L_{total} = Min(L_{rad}, L_N, L_{Si}) \quad (B26)$$

[46] In the nutrient L factors inhibition χ must be zero except for nitrate, which competes with the alternate (reduced) form NH_4^+ . The I are radiation intensities which we carry in units of W/m^2 .

[47] Several processes are modeled in a primitive fashion as cumulative or nested routings of the integrated nitrogen growth. Examples include respiration (Res), grazing (Gra), assimilation (As) of biomass into the zooplankton, spillage (Sp) during the consumption process, and excretion (Ex) by the zooplankton. Senescence, by contrast, has its own temperature dependence and tracks ice algal population. Simultaneously it drives the ultimate material remineralization. Here the factors are mortality (M) as a mirror for nitrogen growth and remineralization (Rem) of the detritus.

$$\begin{aligned} \text{Res}^{\text{bot}} &= f_{\text{res}} G^{\text{bot}}, \quad \text{Gra}^{\text{bot}} = f_{\text{gra}} G^{\text{bot}}, \quad \text{Sp}^{\text{bot}} = f_{\text{sp}} \text{Gra}^{\text{bot}}, \\ \text{As}^{\text{bot}} &= f_{\text{as}} \text{Gra}^{\text{bot}}, \quad \text{Ex}^{\text{bot}} = f_{\text{ex}} \text{As}^{\text{bot}} \end{aligned} \quad (\text{B27})$$

$$f_{\text{res}} + f_{\text{gra}} \leq 1, \quad f_{\text{sp}} + f_{\text{as}} = 1, \quad f_{\text{ex}} \leq 1 \quad (\text{B28})$$

$$M^{\text{bot}} = m_{\text{pre}} e^{m_{\text{exp}} C^{\text{v}}} N_{\text{al}}^{\text{bot}}, \quad \text{Rem}^{\text{bot}} = f_{\text{rem}} M^{\text{bot}} \quad (\text{B29})$$

Note that biomass is conserved over spillage and assimilation. In the interest of maintaining clarity, many of the fractionations have been written out explicitly in the above concentration derivatives.

[48] Removal of algae from the bottom ice volume may be caused by flushing or else by sloughing during the melt. In the current study, sensitivity testing has been devoted to discrimination of the respective loss portions but they remain very uncertain. Here the change in h_{me} is the bottom thickness ablated during a time step.

$$F_{\text{al}} = \left(f_{\text{fl}} v_{\text{flush}} + f_{\text{me}} \left(\frac{\Delta h_{\text{me}}}{\Delta t} \right) \right) T_{\text{al}}^{\text{bot}} \quad (\text{B30})$$

Ice-sulfur redox chemistry begins with in vivo synthesis of a complex precursor chain, building from seawater sulfate and eventually leading to amino acids and lipids. The key ingredient, however, is the osmolyte/cryoprotectant DMSP_p. Along with pigments and the cell carbon content, its levels are set proportional to ice algal nitrogen. DMSP_d enters solution directly along all cell disruption pathways, but with additional switches superimposed to provide flexibility. In the excretion channel, for instance, $(1 - f_{\text{ex}2\text{S}})$ can be held in reserve in order to remove S atoms into the hypothetical zooplankton bin. Otherwise, the basic nitrogen forms just recur under multiplication by $R_{\text{S}2\text{N}}$. Examples include

$$\text{Sp}_{\text{DMSP}_d}^{\text{bot}} = R_{\text{S}2\text{N}}^{\text{bot}} \text{Sp}^{\text{bot}} = R_{\text{S}2\text{N}}^{\text{bot}} f_{\text{sp}} \text{Gra}^{\text{bot}} = R_{\text{S}2\text{N}}^{\text{bot}} f_{\text{sp}} f_{\text{gra}} G^{\text{bot}} \quad (\text{B31})$$

$$\text{Ex}_{\text{DMSP}_d}^{\text{bot}} = R_{\text{S}2\text{N}}^{\text{bot}} f_{\text{ex}2\text{S}} f_{\text{ex}} f_{\text{as}} f_{\text{gra}} G^{\text{bot}} \quad (\text{B32})$$

in which the terms are now subscripted because they are out-of-currency, and the opportunity is taken to show some of the routing cascades written out in full. Beyond the disruption steps, sulfur kinetics merely constitute the familiar A goes to B etc. of conversion (Con) followed by oxidation (Ox). In

these cases yield applies only to the production of dimethyl sulfide, not to net DMSP_d loss.

$$\text{Con}_S^{\text{bot}} = Y_{\text{con}} k_{\text{con}} \text{DMSP}_d^{\text{bot}}, \quad \text{Ox}_S^{\text{bot}} = k_{\text{ox}} \text{DMSP}_d^{\text{bot}} \quad (\text{B33})$$

Sulfur solutes exchange into the product layer via flux equations identical to those outlined for the dissolved nutrients, except that T^{pr} must be substituted for T^{ml} . A short-circuit into the “pr” volume is provided for ice bottom DMSP_p, which is permitted to enter as DMSP_d released from flushed or ablated detritus. Finally in order to enhance comparisons with the rare data, a supplemental flow is associated with fixed below-ice chlorophyll. Local introduction and removal inside the product bin may then be summarized as

$$\text{Slo}_{\text{DMSP}_d}^{\text{pr}} = R_{\text{S}2\text{N}}^{\text{bot}} f_{\text{rtr}} \left(\frac{F_{\text{al}}}{I_{\text{pr}}} \right) \quad (\text{B34})$$

$$\text{Bkg}_{\text{DMSP}_d}^{\text{pr}} = k_{\text{dis}} \left(\frac{R_{\text{S}2\text{N}}^{\text{pr}}}{R_{\text{Chl}2\text{N}}^{\text{pr}}} \right) \text{Chl}_{\text{al}}^{\text{pr}} = k_{\text{dis}} \text{DMSP}_p^{\text{pr}} \quad (\text{B35})$$

$$\text{Con}_S^{\text{pr}} = Y_{\text{con}} k_{\text{con}} \text{DMSP}_d^{\text{pr}}, \quad \text{Ox}_S^{\text{pr}} = k_{\text{ox}} \text{DMSP}_d^{\text{pr}}, \quad (\text{B36})$$

where Slo and Bkg are the distinct sloughing and background sources. Subscript rtr stands for return from sinking detritus, and dis indicates cell disruption of some type (grazing, senescence or others).

[49] **Acknowledgments.** The authors would like to thank the U.S. Department of Energy Scientific Discovery through Advanced Computing (SciDAC) Program and the Experimental Program to Stimulate Competitive Research (EPSCoR) for support of this project (grant DE-FG02-08ER46502).

References

- Andreae, M. O., and A. R. Rosenfeld (2008), Aerosol-cloud-precipitation interactions Part I. The nature and sources of cloud active aerosols, *Earth Sci. Rev.*, **89**, 13–41, doi:10.1016/j.earscirev.2008.03.001.
- Archer, S. D., F. J. Gilbert, J. I. Allen, J. Blackford, and P. D. Nightingale (2004), Modelling of the seasonal patterns of dimethylsulphide production and fate during 1989 at a site in the North Sea, *Can. J. Fish. Aquat. Sci.*, **61**, 765–787, doi:10.1139/f04-028.
- Arrigo, K. R. (2003), Primary production in sea ice, in *Sea Ice: An Introduction to its Physics, Chemistry, Biology and Geology*, edited by D. N. Thomas and G. S. Dieckmann, pp. 143–183, Blackwell, London.
- Arrigo, K. R., and D. Thomas (2004), Large scale importance of sea ice biology in the Southern Ocean, *Antarct. Sci.*, **16**, 471–486, doi:10.1017/S0954102004002263.
- Arrigo, K. R., J. N. Kremer, and C. W. Sullivan (1993), A simulated Antarctic fast ice ecosystem, *J. Geophys. Res.*, **98**(C4), 6929–6946, doi:10.1029/93JC00141.
- Bitz, C. M., and W. H. Lipscomb (1999), An energy-conserving thermodynamic model of sea ice, *J. Geophys. Res.*, **104**(C7), 15,669–15,677, doi:10.1029/1999JC900100.
- Briegleb, B. P., C. M. Bitz, E. C. Hunke, W. H. Lipscomb, M. M. Holland, J. L. Schramm, and R. E. Moritz (2004), Scientific description of the sea ice component in the Community Climate System Model, Version 3, *Tech. Rep. NCAR/TN-463+STR*, Natl. Cent. for Atmos. Res., Boulder, Colo. [Available at <http://nldr.library.ucar.edu/repository/collections/TECH-NOTE-000-000-000-535>]
- Carmack, E., and P. Wassman (2006), Food webs and physical-biological coupling on pan-Arctic shelves: Unifying concepts and comprehensive perspectives, *Prog. Oceanogr.*, **71**, 446–447.
- Charlson, R. J., J. E. Lovelock, M. O. Andreae, and S. G. Warren (1987), Oceanic phytoplankton, atmospheric sulphur, cloud albedo and climate, *Nature*, **326**, 655–661, doi:10.1038/326655a0.
- Collins, W. D., et al. (2006), The Community Climate System Model Version 3 (CCSM3), *J. Clim.*, **19**, 2122–2143, doi:10.1175/JCLI3761.1.

- Conkright, M. E., H. E. Garcia, T. D. O'Brien, R. A. Locarnini, T. P. Boyer, C. Stephens, and J. I. Antonov (2002), *Nutrients*, vol. 4, *NOAA Atlas NESDIS*, NOAA, Silver Spring, Md.
- Cota, G. F., and E. P. W. Horne (1989), Physical control of arctic ice algal production, *Mar. Ecol. Prog. Ser.*, **52**, 111–121, doi:10.3354/meps052111.
- Deal, C., M. Jin, S. Elliott, E. Hunke, M. Maltrud, and N. Jeffery (2011), Large-scale modeling of primary production and ice algal biomass within arctic sea ice in 1992, *J. Geophys. Res.*, **116**, C07004, doi:10.1029/2010JC006409.
- Elliott, S. (2009), Dependence of DMS global sea-air flux distribution on transfer velocity and concentration field type, *J. Geophys. Res.*, **114**, G02001, doi:10.1029/2008JG000710.
- Ferek, R. J., P. V. Hobbs, L. F. Radke, J. A. Herring, W. T. Sturges, and G. F. Cota (1995), Dimethyl sulfide in the arctic atmosphere, *J. Geophys. Res.*, **100**(D12), 26,093–26,104, doi:10.1029/95JD02374.
- Gosselin, M., L. Legendre, J.-C. Theriault, and S. Demers (1990), Light and nutrient limitation of sea-ice microalgae (Hudson Bay, Canadian Arctic), *J. Phycol.*, **26**, 220–232, doi:10.1111/j.0022-3646.1990.00220.x.
- Gosselin, M., M. Levasseur, P. A. Wheeler, R. A. Horner, and B. C. Booth (1997), New measurements of phytoplankton and ice algal production in the Arctic Ocean, *Deep Sea Res., Part II*, **44**, 1623–1644, doi:10.1016/S0967-0645(97)00054-4.
- Gradinger, R. (1999), Vertical fine structure of the biomass and composition of algal communities in Arctic pack ice, *Mar. Biol. Berlin*, **133**, 745–754, doi:10.1007/s002270050516.
- Gradinger, R. (2009), Sea-ice algae: Major contributors to primary production and algal biomass in the Chukchi and Beaufort seas during May/June, *Deep Sea Res., Part II*, **56**(17), 1201–1212, doi:10.1016/j.dsr2.2008.10.016.
- Gradinger, R., K. Meiners, G. Plumley, Q. Zhang, and B. Bluhm (2005), Abundance and composition of the sea-ice meiofauna in off-shore pack ice of the Beaufort Gyre in summer 2002 and 2003, *Polar Biol.*, **28**, 171–181, doi:10.1007/s00300-004-0674-5.
- Gunst, R. F., and R. L. Mason (1980), *Regression Analysis and its Applications*, Marcel Dekker, New York.
- HAAO (2001), *Hydrochemical Atlas of the Arctic Ocean*, Int. Arctic Res. Cent., Fairbanks, Alaska.
- Hellmer, H. H., M. Schröder, C. Haas, G. S. Dieckmann, and M. Spindler (2008), The ISPOL drift experiment, *Deep Sea Res., Part II*, **55**, 913–917, doi:10.1016/j.dsr2.2008.01.001.
- Hunke, E. C. (2010), Thickness sensitivities in the CICE sea ice model, *Ocean Modell.*, **34**, 137–149, doi:10.1016/j.ocemod.2010.05.004.
- Hunke, E. C., and C. M. Bitz (2009), Age characteristics in a multidecadal Arctic sea ice simulation, *J. Geophys. Res.*, **114**, C08013, doi:10.1029/2008JC005186.
- Hunke, E. C., and J. K. Dukowicz (1997), An elastic-viscous-plastic model for sea ice dynamics, *J. Phys. Oceanogr.*, **27**, 1849–1867, doi:10.1175/1520-0485(1997)027<1849:AEVPMF>2.0.CO;2.
- Hunke, E. C., and W. H. Lipscomb (2008), CICE: The Los Alamos sea ice model documentation and software user's manual, Version 4.0, *Tech. Rep. LA-CC-06-012*, Los Alamos Natl. Lab., Los Alamos, N. M.
- Irwin, B. D. (1990), Primary production of ice algae on a seasonally ice covered continental shelf, *Polar Biol.*, **10**, 247–254, doi:10.1007/BF00238421.
- Jin, M., C. J. Deal, J. Wang, K.-H. Shin, N. Tanaka, T. E. Whitledge, S. H. Lee, and R. Gradinger (2006), Controls of the land fast ice-ocean ecosystem offshore Barrow, Alaska, *Ann. Glaciol.*, **44**, 63–72, doi:10.3189/172756406781811709.
- Kettle, A. J., and M. O. Andreae (2000), Flux of dimethylsulfide from the oceans: A comparison of updated data sets and flux models, *J. Geophys. Res.*, **105**(D22), 26,793–26,808, doi:10.1029/2000JD900252.
- Kiene, R. P., and T. S. Bates (1990), Biological removal of dimethyl sulfide from sea water, *Nature*, **345**, 702–705, doi:10.1038/345702a0.
- Kiene, R. P., and D. Slezak (2006), Low dissolved DMSP concentrations in seawater revealed by small-volume gravity filtration and dialysis sampling, *Limnol. Oceanogr. Methods*, **4**, 80–95, doi:10.4319/lom.2006.4.80.
- Kiene, R. P., L. J. Linn, and J. A. Bruton (2000), New and important roles for DMSP in marine microbial communities, *J. Sea Res.*, **43**, 209–224, doi:10.1016/S1385-1101(00)00023-X.
- Krembs, C., R. Gradinger, and M. Spindler (2000), Implications of brine channel geometry and surface area for the interaction of sympagic organisms in Arctic sea ice, *J. Exp. Mar. Biol. Ecol.*, **243**, 55–80, doi:10.1016/S0022-0981(99)00111-2.
- Kudoh, S., B. Robineau, Y. Suzuki, Y. Fujiyoshi, and M. Takahashi (1997), Photosynthetic acclimation and the estimation of temperate ice algal primary production in Saroma-ko Lagoon, Japan, *J. Mar. Syst.*, **11**, 93–109, doi:10.1016/S0924-7963(96)00031-0.
- Lannuzel, D., V. Schoemann, J. de Jong, L. Chou, B. Delille, S. Becquevort, and J. L. Tison (2007), Distribution and biogeochemical behavior of iron in East Antarctic sea ice, *Mar. Chem.*, **106**, 18–32, doi:10.1016/j.marchem.2006.06.010.
- Lavoie, D., K. Denman, and C. Michel (2005), Modeling ice algal growth and decline in a seasonally ice-covered region of the Arctic (Resolute Passage, Canadian Archipelago), *J. Geophys. Res.*, **110**, C11009, doi:10.1029/2005JC002922.
- Lavoie, D., R. W. Macdonald, and K. L. Denman (2009), Primary productivity and export fluxes on the Canadian shelf of the Beaufort Sea: A modeling study, *J. Mar. Syst.*, **75**, 17–32, doi:10.1016/j.jmarsys.2008.07.007.
- Leck, C., and C. Persson (1996), The central Arctic Ocean as a source of dimethyl sulfide: Seasonal variability in relation to biological activity, *Tellus, Ser. B*, **48**, 156–177, doi:10.1034/j.1600-0889.1996.t01-1-00003.x.
- Le Clainche, Y., et al. (2010), A first appraisal of prognostic ocean DMS models and prospects for their use in climate models, *Global Biogeochem. Cycles*, **24**, GB3021, doi:10.1029/2009GB003721.
- Lee, P. A., S. J. de Mora, M. Gosselin, M. Levasseur, R. C. Bouillon, C. Nozais, and C. Michel (2001), Particulate dimethylsulfoxide in Arctic sea ice algal communities: The cryoprotectant hypothesis revisited, *J. Phycol.*, **37**, 488–499, doi:10.1046/j.1529-8817.2001.037004488.x.
- Levasseur, M., M. Gosselin, and S. Michaud (1994), New source of dimethylsulfide (DMS) for the arctic atmosphere: Ice diatoms, *Mar. Biol. Berlin*, **121**, 381–387, doi:10.1007/BF00346748.
- Lipscomb, W. H., and E. C. Hunke (2004), Modeling sea ice transport using incremental remapping, *Mon. Weather Rev.*, **132**, 1341–1354, doi:10.1175/1520-0493(2004)132<1341:MSITU>2.0.CO;2.
- Lipscomb, W. H., E. C. Hunke, W. Maslowski, and J. Jakacki (2007), Ridging, strength, and stability in high-resolution sea ice models, *J. Geophys. Res.*, **112**, C03S91, doi:10.1029/2005JC003355.
- Lundén, J., G. Svensson, and C. Leck (2007), Influence of meteorological processes on the spatial and temporal variability of atmospheric dimethyl sulfide in the high Arctic summer, *J. Geophys. Res.*, **112**, D13308, doi:10.1029/2006JD008183.
- Matrai, P., M. Vernet, and P. Wassmann (2007), Relating temporal and spatial patterns of DMSP in the Barents Sea to phytoplankton biomass and productivity, *J. Mar. Syst.*, **67**, 83–101, doi:10.1016/j.jmarsys.2006.10.001.
- Matrai, P. A., L. Tranvik, C. Leck, and J. C. Knulst (2008), Are high arctic surface microlayers a potential source of aerosol precursors? *Mar. Chem.*, **108**, 109–122, doi:10.1016/j.marchem.2007.11.001.
- Meehl, J., et al. (2007), Global climate projections, in *Climate Change 2007: The Physical Science Basis. Contribution of Working Group I to the Fourth Assessment Report of the Intergovernmental Panel on Climate Change*, edited by S. Solomon et al., pp. 789–844, Cambridge Univ. Press, Cambridge, U. K.
- Michaud, S., M. Levasseur, and G. Cantin (2007), Seasonal variations in dimethyl sulfoniopropionate and dimethylsulfide concentrations in relation to the plankton community in the St. Lawrence Estuary, *Estuarine Coastal Shelf Sci.*, **71**, 741–750, doi:10.1016/j.ecss.2006.09.020.
- Michel, C., L. Legendre, R. G. Ingram, M. Gosselin, and M. Levasseur (1996), Carbon budget of sea-ice algae in spring: Evidence of a significant transfer to zooplankton grazers, *J. Geophys. Res.*, **101**(C8), 18,345–18,360, doi:10.1029/96JC00045.
- Monfort, P., S. Demers, and M. Levasseur (2000), Bacterial dynamics in first-year sea ice and underlying seawater of Saroma-ko Lagoon and Resolute Passage: Inhibitory effects of ice algae on bacterial dynamics, *Can. J. Microbiol.*, **46**, 623–632, doi:10.1139/w00-024.
- Niedrauer, T. M., and S. Martin (1979), An experimental study of brine drainage and convection in young sea ice, *J. Geophys. Res.*, **84**(C3), 1176–1186, doi:10.1029/JC084iC03p01176.
- Reeburgh, W. (1984), Fluxes associated with brine motion in growing sea ice, *Polar Biol.*, **3**, 29–33, doi:10.1007/BF00265564.
- Rysgaard, S., J. Bendtsen, L. T. Pedersen, H. Ramløv, and R. N. Glud (2009), Increased CO₂ uptake due to sea ice growth and decay in the Nordic Seas, *J. Geophys. Res.*, **114**, C09011, doi:10.1029/2008JC005088.
- Saiz-Lopez, A., A. Mahajan, R. A. Salmon, S. J. B. Bauguette, A. E. Jones, H. K. Roscoe, and J. C. Plane (2007), Boundary layer halogens in coastal Antarctica, *Science*, **317**, 348–351, doi:10.1126/science.1141408.
- Schlosser, P., J. H. Swift, D. Lewis, and S. L. Pfirman (1995), Role of the large scale Arctic Ocean circulation in the transport of contaminants, *Deep Sea Res., Part II*, **42**, 1341–1367, doi:10.1016/0967-0645(95)00045-3.
- Sharma, S., L. A. Barrie, D. Plummer, J. C. McConnell, P. C. Brickell, M. Levasseur, M. Gosselin, and T. S. Bates (1999), Flux estimation of oceanic dimethyl sulfide around North America, *J. Geophys. Res.*, **104**(D17), 21,327–21,342, doi:10.1029/1999JD900207.

- Smith, R. E. H., W. G. Harrison, L. R. Harris, and A. W. Herman (1990), Vertical fine structure of particulate matter and nutrients in sea ice of the high Arctic, *Can. J. Fish. Aquat. Sci.*, **47**, 1348–1355, doi:10.1139/f90-154.
- Stefels, J. (2000), Physiological aspects of the production and conversion of DMSP in marine algae and higher plants, *J. Sea Res.*, **43**, 183–197, doi:10.1016/S1385-1101(00)00030-7.
- Stefels, J., M. Steinke, S. Turner, G. Malin, and S. Belviso (2007), Environmental constraints on the production and removal of the climatically active gas dimethylsulphide (DMS), *Biogeochemistry*, **83**, 245–275, doi:10.1007/s10533-007-9091-5.
- Suzuki, Y., S. Kudoh, and M. Takahashi (1997), Photosynthetic and respiratory characteristics of an Arctic ice algal community living in low light and low temperature conditions, *J. Mar. Syst.*, **11**, 111–121, doi:10.1016/S0924-7963(96)00032-2.
- Uzuka, N. (2003), A time series observation of DMSP production in the fast ice zone near Barrow, *Sci. Rep. Tohoku Univ., Ser. 5*, **36**, 439–442.
- Vallina, S. M., R. Simó, T. R. Anderson, A. Gabric, R. Cropp, and J. M. Pacheco (2008), A dynamic model of oceanic sulfur (DMOS) applied to the Sargasso Sea: Simulating the dimethylsulfide (DMS) summer paradox, *J. Geophys. Res.*, **113**, G01009, doi:10.1029/2007JG000415.
- Vancoppenolle, M., H. Goosse, A. de Montety, T. Fichet, B. Tremblay, and J.-L. Tison (2010), Modeling brine and nutrient dynamics in Antarctic sea ice: The case of dissolved silica, *J. Geophys. Res.*, **115**, C02005, doi:10.1029/2009JC005369.
- Wakatsuchi, M., and N. Ono (1983), Measurements of salinity and volume of brine excluded from growing sea ice, *J. Geophys. Res.*, **88**(C5), 2943–2951, doi:10.1029/JC088iC05p02943.
- Werner, I., J. Ivalko, and H. Schunemann (2007), Sea-ice algae in Arctic pack ice during late winter, *Polar Biol.*, **30**, 1493–1504, doi:10.1007/s00300-007-0310-2.
- Zar, J. H. (1984), *Biostatistical Analysis*, Prentice Hall, Upper Saddle River, N. J.
- Zhou, J., E. Swietlicki, O. H. Berg, P. P. Aalto, K. Hämeri, E. D. Nilsson, and C. Leck (2001), Hygroscopic properties of aerosol particles over the central Arctic Ocean during summer, *J. Geophys. Res.*, **106**(D23), 32,111–32,123, doi:10.1029/2000JD900426.
- C. Deal and M. Jin, International Arctic Research Center, Institute of Marine Science, University of Alaska Fairbanks, Fairbanks, AK 99775-7340, USA.
- S. Elliott, E. Hunke, and N. Jeffery, Climate Ocean Sea Ice Modeling, Computational Sciences Division, Los Alamos National Laboratory, Mail Stop D-413, Los Alamos, NM 87545, USA. (sme@lanl.gov)
- G. Humphries, Institute of Arctic Biology, University of Alaska Fairbanks, Fairbanks, AK 99775, USA.
- M. Levasseur, Department of Biology, Laval University, 1045, Avenue de la Médecine, Pavillon Alexandre-Vachon, Quebec, QC G1V 0A6, Canada.
- J. Stefels, Laboratory of Plant Physiology, Center for Life Sciences, University of Groningen, Bldg. 5173, Nijenborgh 7, NL-9747 AG Groningen, Netherlands.